Description and application of a budget-diagnosis tool in COSMO

WOLFGANG LANGHANS[1], OLIVER FUHRER[2], AND JÜRG SCHMIDLI[1]

[1] *Institute for Atmospheric and Climate Science, ETH Zurich, Switzerland*

[2] *Federal Office of Meteorology and Climatology MeteoSwiss, Switzerland*

1 Introduction

A budget analysis tool has been implemented into the code of the non-hydrostatic COSMO model in order to diagnose both temperature and moisture tendencies. The implementation allows for the extraction of both physical and dynamical tendencies of either temperature or potential temperature and of moisture scalars. Application of this tool may serve different purposes ranging from numerical developments to process studies and climate science.

A brief description of the retrieval of tendencies is given here and the applied method is exemplified by two simulations. Firstly, an idealized rising warm-bubble test (Wicker and Skamarock 1998) is conducted to explain the underlying temperature tendencies. Secondly, erroneous cold-pool formation in a real-case simulation is studied and the cause for unrealistic cold temperatures will be determined from the budget analysis. As will be demonstrated, the split-explicit time-stepping applied in COSMO complicates the diagnosis of temperature advection tendencies. A further complication is introduced by the COSMO option of solving the heat equation either for temperature or potential temperature. Moisture tendencies related to advection can be obtained much more easily, since the moisture tendencies are numerically solved using discretization schemes without mode-splitting (e.g., a positive-definite scheme).

2 COSMO heat budget

Derived from the first law of thermodynamics the temperature equation solved in COSMO is given as

$$\frac{\partial T}{\partial t} = ADV_T + \frac{1}{\rho c_{pd}}\frac{dp}{dt} + M_L + M_T + M_C + M_{SSO} + M_R + M_{HD} + M_{RLX}. \quad (1)$$

The terms on the right hand side are the heating terms due to advection, pressure changes, latent heating M_L, turbulent flux divergence $M_T = -\frac{1}{\rho c_{pd}}\nabla \cdot \mathbf{H}$, parameterized convection M_C, parameterized drag due to subgrid-orography M_{SSO}, radiative flux divergence M_R, computational mixing M_{HD}, and relaxation at lateral and top boundaries M_{RLX}. The advective tendency is written as

$$ADV_T = -\underbrace{\left[\frac{1}{a\cos(\varphi)}\left(u\frac{\partial T'}{\partial \lambda} + v\cos(\varphi)\frac{\partial T'}{\partial \varphi}\right)\right]}_{HADV_{T'}} - \dot{\zeta}\frac{\partial T'}{\partial \zeta} - w\frac{dT_0}{dz}. \quad (2)$$

Here λ, φ, and ζ are the transformed coordinates. Primes indicate deviations from the model's base-state temperature $T_0(z)$, HADV$_{T'}$ is the horizontal advection of T', ρ is the

density of air, and a is the Earth's radius. Alternatively, a potential temperature equation can be solved in COSMO (namelist options `itheta_adv=1,2`), given as

$$\frac{\partial \theta}{\partial t} = ADV_\theta + \frac{\theta}{T} M_\Sigma \tag{3}$$

$$ADV_\theta = \underbrace{-\left[\frac{1}{a\cos(\varphi)} \left(u\frac{\partial \Phi}{\partial \lambda} + v\cos(\varphi)\frac{\partial \Phi}{\partial \varphi} \right) \right]}_{HADV_\Phi} - \dot{\zeta}\frac{\partial \Phi}{\partial \zeta} - \begin{cases} w\frac{d\theta_0}{dz} & \text{for} \quad \Phi = \theta' \\ 0 & \text{for} \quad \Phi = \theta \end{cases} \tag{4}$$

with M_Σ an abbreviation for all diabatic temperature tendencies introduced above. Thereby, advection can be computed for either $\Phi = \theta$ or $\Phi = \theta'$. All temperature tendencies in Eqs. (1) and (3) are evaluated at mass points.

The adiabatic part of the temperature equation is solved using a time-splitting method (Wicker and Skamarock 2002). Thereby, terms related to acoustic and gravity-wave propagation are typically solved implicitly on smaller timesteps. In COSMO the term related to the total derivative of pressure (see Eq. (1)) and the vertical advection of the temperature base-state T_0 (alternatively θ_0) (last terms in Eqs. (2) and (4)) are solved on small timesteps, while the remaining advective tendencies are evaluated on Runge-Kutta substeps (see also Gassmann and Herzog 2007). In case of $\Phi = \theta$ the complete temperature equation is solved on Runge-Kutta substeps without fast-mode contributions. In total three different formulations are available in COSMO to solve the heat equation using Runge-Kutta time-integration (see also Tab. **??**). All other M terms are computed as slow processes outside the Runge-Kutta integration.

`itheta_adv`	0	1	2
equation for	T'	θ'	θ
fast-mode	$\frac{1}{\rho c_{pd}}\frac{dp}{dt} - w\frac{dT_0}{dz}$	$-w\frac{d\theta_0}{dz}$	-
slow-mode	$HADV_{T'} - \dot{\zeta}\frac{\partial T'}{\partial \zeta}$	$HADV_{\theta'} - \dot{\zeta}\frac{\partial \theta'}{\partial \zeta}$	$HADV_\theta - \dot{\zeta}\frac{\partial \theta}{\partial \zeta}$

Table 1: Overview of three different available methods (set by namelist switch `itheta_adv`=0–2) for solving the temperature equation in COSMO. For each option the dynamic temperature tendencies computed on small and large timesteps (i.e., Runge-Kutta substeps) are indicated. Note that in any case diabatic tendencies M_Σ are computed outside the Runge-Kutta integration.

An implicit Crank-Nicholson discretization is applied in the fast-wave solver. This results in a time-averaged equation for the updated temperature (either T or θ) after one small timestep $\Delta\tau$, given in case of 2nd-order accurate differencing as

$$T_k^{\nu+1} = T_k^\nu + (f_T^n)_k \Delta\tau \tag{5}$$

$$\underbrace{-\frac{p_k^n}{c_{vd}\rho_k^n}(D_h^{\nu+1})_k \Delta\tau + \frac{C_k^{p1}}{c_{pd}\rho_k^n}\left\{ \beta^-(w_{k+1}^\nu - w_k^\nu) + \beta^+(w_{k+1}^{\nu+1} - w_k^{\nu+1}) \right\}}_{\frac{1}{\rho c_{pd}}\frac{dp}{dt}} \tag{6}$$

$$\underbrace{-\frac{dT_0}{dz}(\beta^-\overline{w^\nu}_k^\zeta + \beta^+\overline{w^{\nu+1}}_k^\zeta)}_{T_0-\text{advection}}. \tag{7}$$

Here $(f_T^n)_k$ corresponds to the slow-mode tendencies at time step n and level k, which are kept constant during all Runge-Kutta stages, and $(D_h^{\nu+1})_k$ is the horizontal divergence. Detailed information on the fast-mode discretization and the notation is given in the COSMO documentation (Doms and Schättler 2002, pp. 64–68). In COSMO the total derivative of pressure

consists only of the divergence term (6); the effects from diabatic heating are neglected. In more sophisticated cloud models these effects are included. As mentioned earlier, the advection of the temperature base-state (7) is computed for T' and θ' advection (`itheta_adv=0,1`).

To diagnose the complete advective tendencies the fast-mode advection is accumulated over all small timesteps during the final Runge-Kutta stage and added to the slow-mode advective tendencies. Since the pressure tendency term in (1) is not computed in case of a θ formulation (`itheta_adv=1--2`), the temperature advection can not be obtained from potential temperature advection in these cases. The other way round, in case of T'-advection (`itheta_adv=0`) the potential temperature advection can be diagnosed at the end of each large timestep as the difference of net potential temperature tendency and diabatic tendencies. To summarize, while advective θ tendencies can be retrieved for `itheta_adv=0--2`, T advection is only diagnosable in case of `itheta_adv=0`.

Moreover, for optimal physical interpretation of advective tendencies, the horizontal and vertical components should be related to advection in physical space, not transformed space. Thus, vertical advection is additionally diagnosed each timestep using second-order centered differences in physical space.

3 COSMO moisture budget

COSMO includes several bulk microphysics parameterizations for grid-scale precipitation. The most complex single-moment formulation (Reinhardt and Seifert 2006) distinguishes between the specific humidity q_v, cloud water q_c, cloud ice q_i, rain water q_r, snow q_s, and graupel q_g, in total six budget equations. To keep the amount of output small, the budget tool diagnoses only the tendencies of two classes of hydrometeors: precipitating ($q_r + q_s + q_g$) and non-precipitating hydrometeors ($q_c + q_i$). Together with the budget of water vapor q_v, three moisture budgets are diagnosed and all involved tendencies are evaluated at mass points. For each class q_x the budget equation can be written as

$$\frac{\partial q_x}{\partial t} = ADV_{qx} + Q_L + Q_T + Q_C + Q_{HD} + Q_{RLX} \tag{8}$$

with advection ADV_{qx}, microphysical exchange processes (including sedimentation) Q_L, turbulent transport Q_T, parameterized convection Q_C, computational mixing Q_{HD}, and relaxation at the domain boundaries Q_{RLX}. All tendencies are computed as slow tendencies outside the RK-dynamics. Thus, the diagnosis of the moisture advection tendencies is not plagued by the complexity introduced by the split-explicit method in case of temperature. Note that COSMO does not compute subgrid-turbulence tendencies for precipitation hydrometeors (thus $Q_T = 0$). The 3D advective tendencies result from either a Semi-Lagrangian (Staniforth and Côté 1991) or a positive-definite (Bott 1989) discretization. As for temperature, truly vertical advection is diagnosed each timestep.

4 Rising bubble test

To illustrate the retrieval of advective tendencies for the three different types of temperature advection a rising warm-bubble simulation is conducted here in two dimensions. The setup closely follows the description given by Wicker and Skamarock (1998). The domain is 20×10 km^2 large and a uniform grid-spacing of 100 m is applied. The long timestep is 2 s and neither computational nor subgrid turbulent diffusion is used. If not mentioned otherwise, horizontal and vertical advection are discretized using a 5th-order upstream scheme and the model's

base-state temperature profile equals a dry neutral stratification with $\theta = 300$ K. The initial thermodynamic conditions are prescribed by a potential temperature disturbance, given as

$$\theta' = 2\cos^2\left(\frac{\pi L}{2}\right) \quad \text{with} \quad L = \sqrt{\left(\frac{x - x_c}{x_r}\right)^2 + \left(\frac{z - z_c}{z_r}\right)^2}, \tag{9}$$

that is added to the dry neutrally stratified atmosphere ($\theta = 300$ K). The disturbance with radius $x_r = z_r = 2$ km is placed at $x_c = 10$ km and $z_c = 2$ km.

Results are analyzed after 1000 s, when the bubble has risen to the center of the domain. The potential temperature and vertical velocity distributions (see Figs. 1a,d) are hardly dependent on the formulation of temperature advection (not shown). All three formulations result in maximum vertical velocities of 14.6 m s^{-1} and maximum θ' perturbations of 2 K and are therefore very similar to results presented using other numerical codes (Wicker and Skamarock 1998; Bryan and Fritsch 2002). However, as a side note, a 2nd-order implicit Crank-Nicholson scheme, which is commonly applied within COSMO for vertical advection, significantly deteriorates the bubbles characteristics (see Figs. 1b,e). A recently developed 3rd-order implicit discretization (see Baldauf 2009) yields considerable improvements (see Figs. 1c,f).
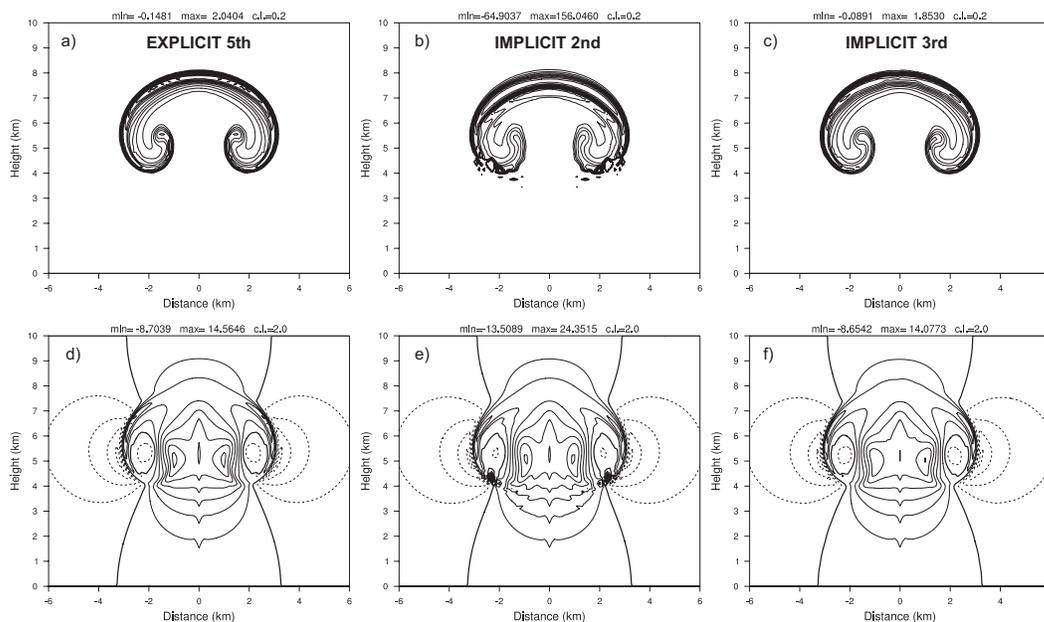
Figure 1: Results of the dry bubble simulation after 1000 s using T'-advection (`itheta_adv=0`): (a–c) Potential temperature perturbation contoured every 0.2 K, (d–f) vertical velocity contoured every 2 m s^{-1}. Vertical T'-advection is computed using (a,d) a 5th-order explicit, (b,e) a 2nd-order implicit scheme, and (c,f) a 3rd-order implicit scheme.

In the following the diagnosis of *potential* temperature tendencies with help of the new implementations is described. Figure 2a shows the net potential temperature tendency, which results from 3D potential temperature advection (see Fig. 2b). Since for this setup the base-state is isentropic the fast-mode tendencies would be zero not only for `itheta_adv=2`, but also for `itheta_adv=1`. The estimated tendencies for vertical advection of θ appear meaningful (see Fig. 2d), as the difference between 3D advection and estimated vertical advection (see Fig. 2e) yields a reasonably good agreement with the actually computed tendencies from horizontal advection, which have also been extracted here (see Fig. 2c).

Finally, the temperature tendencies are studied using `itheta_adv=0`. For the given base-state with $N_0 = 0$ s^{-1} ($\frac{dT_0}{dz} = gc_{pd}^{-1}$) the net temperature tendency (see Fig. 3a) is determined solely
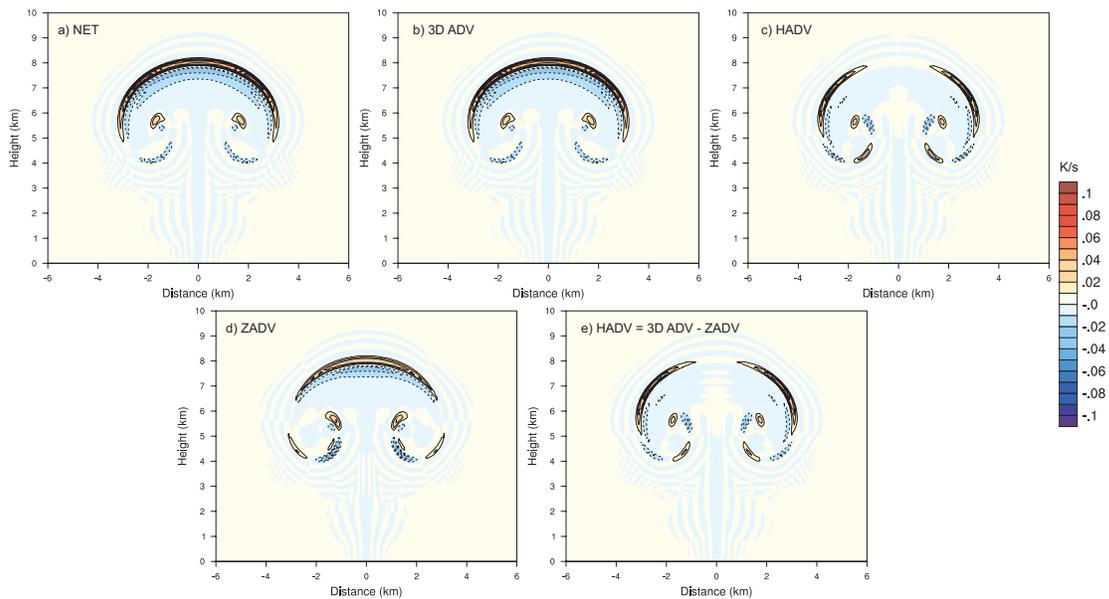
Figure 2: Potential temperature tendencies ($K\,s^{-1}$) obtained after 1000 s using θ-advection (`itheta_adv=2`): (a) Net tendency, (b) 3D advection, (c) horizontal advection, (d) estimated vertical advection, and (e) horizontal advection diagnosed as the difference between full advection and estimated vertical advection.

from advection computed on the Runge-Kutta substeps. The tendencies stemming from the fast-mode solver are negligibly small, as temperature changes due to expansion (see Fig. 3c) and due to base-state advection balance each other in adiabatic ascent to a very high degree. Due to this compensation the sum of total advection and pressure forcing (see Fig. 3e) equals the slow-mode advection without base-state advection (see Fig. 3d). Figure 3f indicates that the total advection is primarily determined by vertical advection. Tendencies from horizontal temperature advection (not shown) are similar to horizontal advection of θ (see Fig. 2c).

A second simulation using a base-state of $N_0 = 0.01$ s^{-1} (not shown) further illustrates the partitioning of fast-mode tendencies into base-state advection and pressure forcing. Since for this setup the temperature profile deviates more strongly from its base-state, the magnitude of the T'-advective tendencies evaluated on Runge-Kutta substeps increases and the fast-mode equilibrium with the pressure forcing is disturbed correspondingly.

5 "Cold-pool" case study

Potential applications of the budget diagnosis tool are manifold. It can be used to further the physical understanding of a specific weather or climate phenomenon as well as to aid model development and problem solution. Here, we present an example of its application to the investigation of the formation of unrealistic cold-pools in steep valleys.

On 11 October 2009 the 12 UTC operational COSMO-2 model run crashed because of a runaway cold-pool in a steep Alpine valley which developed near-surface temperatures below 140 K. Similar events have been observed before and at other locations, but generally the unrealistically low near-surface temperature recovers to normal values after some time. Grid points affected by cold-pools are consistently located within a steep valley which is oriented almost perfectly along the N-S or S-W grid lines. The grid point which exhibits cold-pools most frequently is situated in the Saaser valley and corresponds to a local depression with no outflow (see Fig. 4a).

The 06 UTC COSMO-2 forecast of 5 May 2009 also developed a strong cold-pool in the
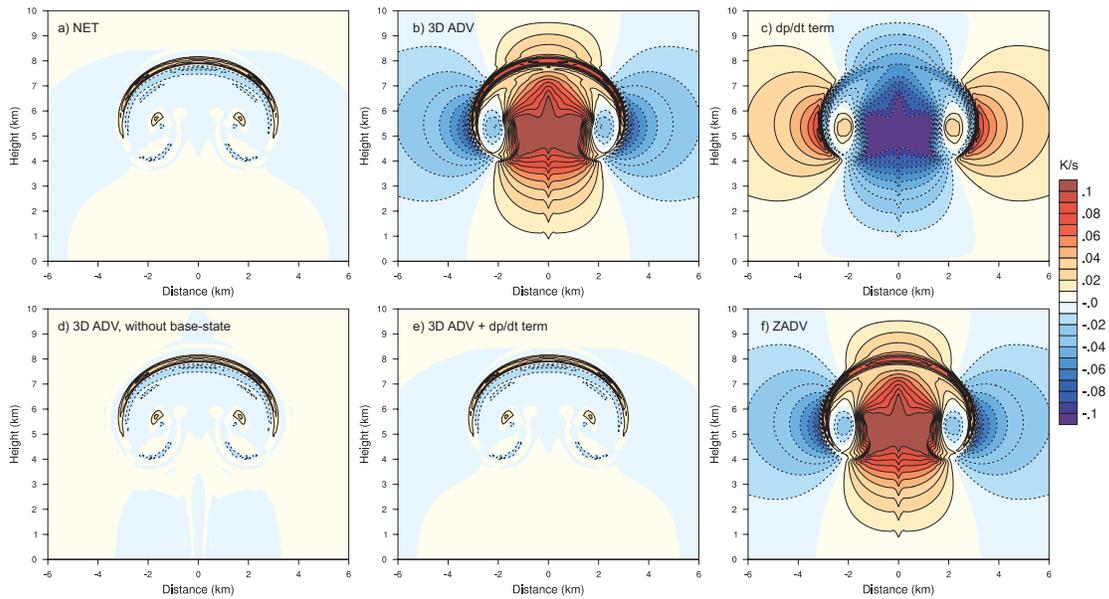
Figure 3: Temperature tendencies (K s^{-1}) obtained after 1000 s using T'-advection (`itheta_adv=0`): (a) Net tendency, (b) 3D advection, (c) $\frac{1}{\rho c_{pd}}\frac{dp}{dt}$ fast-mode term, (d) 3D advection without base-state advection, (e) sum of (b) and (c), and (f) estimated vertical advection.
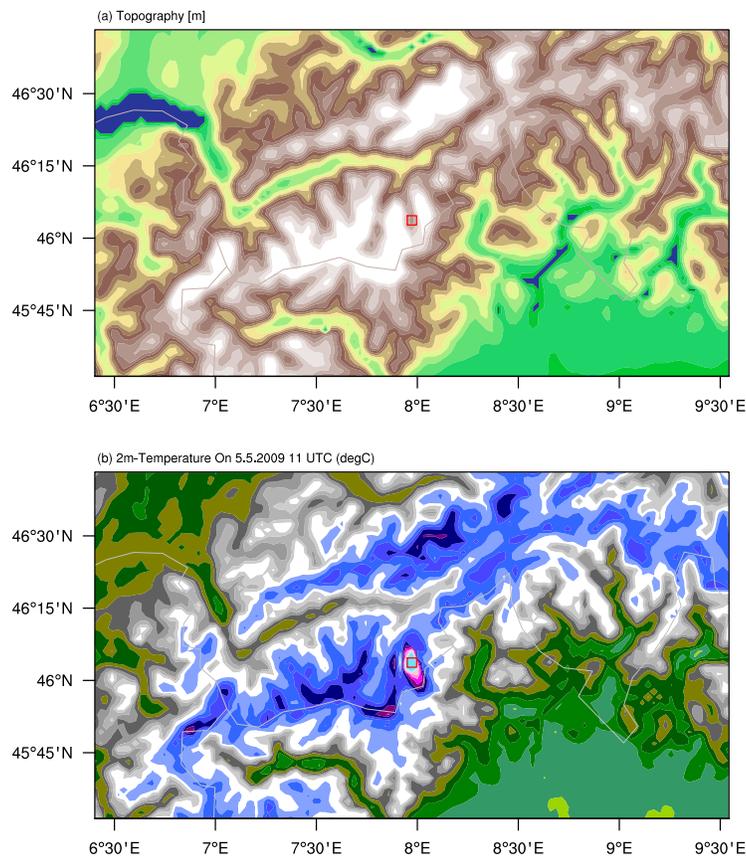
Figure 4: Overview of (a) model topography and (b) 2m-Temperature in °C on 1100 UTC 5 May 2009 after 5 h into the forecast. The grid point with strongest cold-pool development is indicated by a red box.
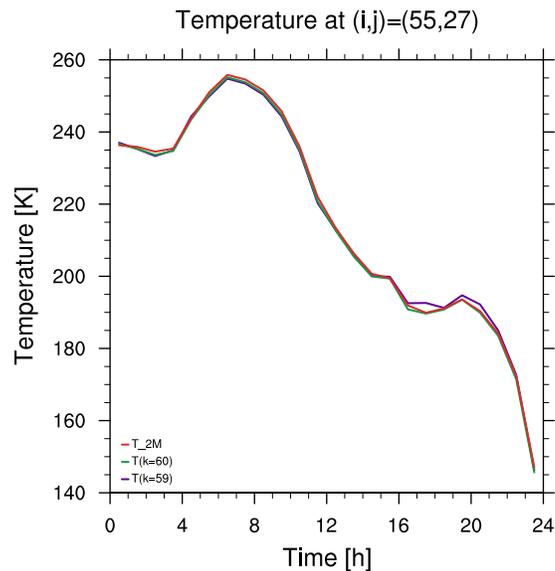
Figure 5: Time series of temperatures at 2 m and on the lowest two model levels (T60, T59).

Saaser valley and is further investigated here. For this event the model did not crash but the cold-pool was unusually persistent and present in over 30 consecutive COSMO-2 forecasts. After 5 h of forecast time (i.e., at 11 UTC) the 2m-temperature distribution (see Fig. 4b) shows a region of unrealistically cold temperatures ($T_{2m} < 243$ K) centered around the lowest valley grid point. Over the course of the simulation temperatures fall below 150 K (see Fig. 5). Later into the simulation, the cold air which accumulated in the Saaser valley spilled into the Rhone valley and deteriorated the forecast quality over a large area.
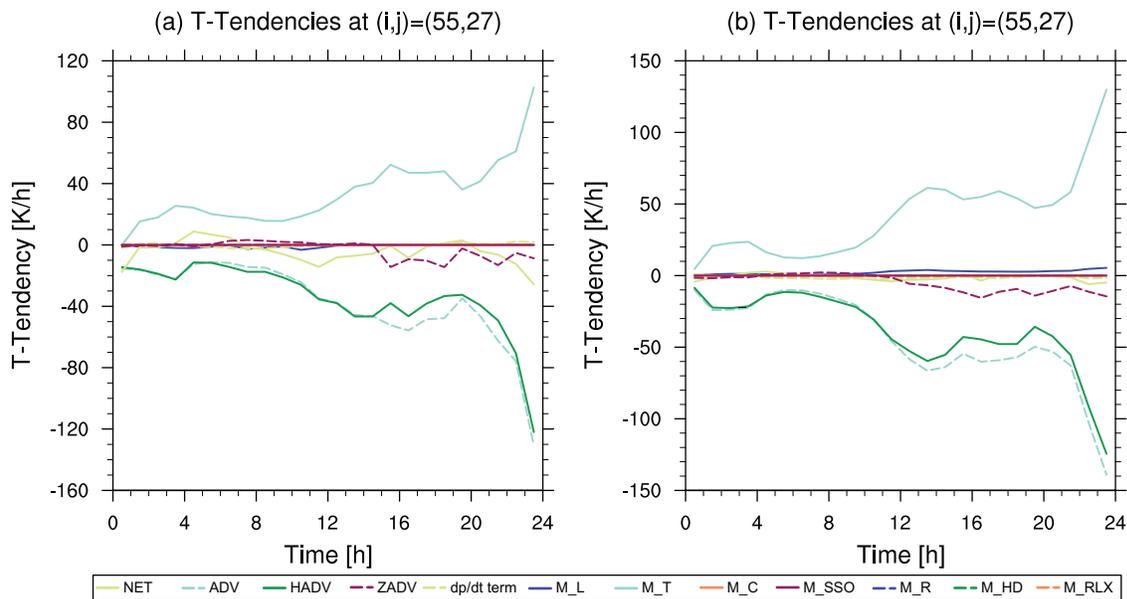
Figure 6: Time series of hourly T-tendencies as determined by the budget diagnosis tool. The budgets are shown for (a) the grid point with lowest temperature and (b) an average over 5x5 grid points around the grid point with lowest temperature.

Further analysis indicates that the forcing responsible for the decreasing temperature does not stem from the surface heat flux, but results from atmospheric cooling that affects the

Earth's surface (not shown). In order to further investigate the source of the forcing, the budget diagnosis tool has been switched on and the simulation repeated. All components of the temperature equation Eq. (1) are shown as hourly averages in Figure 6a. The values shown correspond to the grid point exhibiting the lowest temperatures. The component due to vertical advection (ZADV) has been computed as the difference of the total advective tendency (ADV) and the tendency due to horizontal advection (HADV). The latter results in strong cooling and turbulent diffusion (M_T) counteracts this by mixing with warmer air from higher levels. With the help of the budget diagnosis tool, other processes such as radiative cooling, microphysics, etc. can be excluded from being responsible for the strong cooling. Averaging the tendencies over 5x5 horizontal grid points indicates that this result is robust (see Fig. 6b). Thus, there is a clear indication that in certain topographic configurations the horizontal advection of temperature may introduce a strong spurious forcing leading to the development of cold-pools. This hypothesis is supported by the fact that limiting the temperature advection (`ltadv_limit = .true.`) prevents the cold-pool formation, and that implementing the alternative advection of temperature introduced with model version 4.19 strongly inhibits it.

6 Summary

A budget diagnosis tool has been implemented into COSMO. The implementation allows for the retrieval of heating and moistening rates as computed numerically in the code. Detailed information about the underlying dynamical and physical processes or numerical discretizations can be obtained by studying these tendencies. All tendencies may either be written as instantaneous or as time-averaged quantities. Applications may cover a wide range from model development to process studies at weather and climate scales. Besides the examples provided in this document, the tool has already been applied successfully to study the Alpine heat and moisture budget (Langhans et al. 2011a,b).

References

[1] Baldauf, M. and W. C. Skamarock, 2009: An improved third order vertical advection scheme for the Runge-Kutta dynamical core. *8th International SRNWP-Workshop on Non-Hydrostatic Modelling.*, [Available online at http://www.dwd.de/modellierung].

[2] Bott, A., 1989: A positive definite advection scheme obtained by nonlinear renormalization of the advective fluxes. *Mon. Wea. Rev.*, **117**, 1006–1015.

[3] Bryan, G. H. and J. M. Fritsch, 2002: A benchmark simulation for moist nonhydrostatic numerical models. *Mon. Wea. Rev.*, **130**, 2917–2928.

[4] Doms, G. and U. Schättler, 2002: A description of the nonhydrostatic regional model LM: Part I: Dynamics and Numerics. *Tech. rep.*, [Available online at http://www.cosmomodel.org].

[5] Gassmann, A. and H.-J. Herzog, 2007: A consistent time-split numerical scheme applied to the nonhydrostatic compressible equations. *Mon. Wea. Rev.*, **135**, 20–36

[6] Langhans, W., J. Schmidli, and C. Schär, 2011a: Mesoscale impacts of explicit numerical diffusion in a convection-permitting model. *Mon. Wea. Rev.*, doi:10.1175/2011MWR3650.1

[7] Langhans, W., J. Schmidli, and C. Schär, 2011b: Bulk convergence of cloud-resolving simulations of moist convection over complex terrain. *J. Atmos. Sci.*, submitted.

[8] Reinhardt, T. and A. Seifert, 2006: A three-category ice-scheme for LMK. Tech. rep. *COSMO newsletter*, **6**, 115–120 pp. [Available online at http://www.cosmo-model.org].

[9] Staniforth, A. and J. Côté, 1991: Semi-lagrangian integration schemes for atmospheric models - A review. *Mon. Wea. Rev.*, **119**, 2206–2223.

[10] Wicker L. J. and W. C. Skamarock, 2002: Time-splitting methods for elastic models Using forward time schemes. *Mon. Wea. Rev.*, **130**, 2088–2097.

[11] Wicker L. J. and W. C. Skamarock, 1998: A time-splitting scheme for the elastic equations incorporating second-order Runge-Kutta time differencing. *Mon. Wea. Rev.*, **126**, 1992–199.